5-28-2022

Characteristic Depths, Fluxes, and Timescales for Greenland's Tidewater Glacier Fjords From Subglacial Discharge-Driven Upwelling During Summer

D. A. Slater
The University of Edinburgh

Dustin Carroll
San Jose State University, dustin.carroll@sjsu.edu

H. Oliver
Woods Hole Oceanographic Institution

M. J. Hopwood
Southern University of Science and Technology

F. Straneo
Scripps Institution of Oceanography

See next page for additional authors

Recommended Citation

D. A. Slater, Dustin Carroll, H. Oliver, M. J. Hopwood, F. Straneo, M. Wood, J. K. Willis, and M. Morlighem. "Characteristic Depths, Fluxes, and Timescales for Greenland's Tidewater Glacier Fjords From Subglacial Discharge-Driven Upwelling During Summer" *Geophysical Research Letters* (2022). https://doi.org/10.1029/2021GL097081

Geophysical Research Letters

RESEARCH LETTER
10.1029/2021GL097081

Key Points:

- We present a first ice sheet-wide inventory of subglacial discharge-driven upwelling plumes around the margin of the Greenland Ice Sheet
- Just 0.02 Sv of subglacial discharge drives 0.6–1.6 Sv of upwelling that settles at 0–260 m depth and can renew most fjords within a summer
- Fjords provide a path to the ocean deeper than 200 m for 82 out of 136 glaciers considered, suggesting warm waters reach most major glaciers

Supporting Information:

Supporting Information may be found in the online version of this article.

Correspondence to:

D. A. Slater,
donald.slater@ed.ac.uk

Citation:

Slater, D. A., Carroll, D., Oliver, H., Hopwood, M. J., Straneo, F., Wood, M., et al. (2022). Characteristic depths, fluxes, and timescales for Greenland's tidewater glacier fjords from subglacial discharge-driven upwelling during summer. *Geophysical Research Letters*, *49*, e2021GL097081. https://doi.org/10.1029/2021GL097081

Received 16 NOV 2021
Accepted 25 APR 2022

Characteristic Depths, Fluxes, and Timescales for Greenland's Tidewater Glacier Fjords From Subglacial Discharge-Driven Upwelling During Summer

D. A. Slater[1,2,3], D. Carroll[4,5], H. Oliver[6], M. J. Hopwood[7], F. Straneo[3], M. Wood[5], J. K. Willis[5], and M. Morlighem[8,9]

[1]School of Geosciences, University of Edinburgh, Edinburgh, UK, [2]School of Geography and Sustainable Development, University of St Andrews, St Andrews, UK, [3]Scripps Institution of Oceanography, University of California San Diego, La Jolla, CA, USA, [4]Moss Landing Marine Laboratories, San José State University, San Jose, CA, USA, [5]Jet Propulsion Laboratory, California Institute of Technology, Pasadena, CA, USA, [6]Department of Applied Ocean Physics and Engineering, Woods Hole Oceanographic Institution, Falmouth, MA, USA, [7]Department of Ocean Science and Engineering, Southern University of Science and Technology, Shenzhen, China, [8]Department of Earth Sciences, Dartmouth College, Hanover, NH, USA, [9]Department of Earth System Science, University of California Irvine, Irvine, CA, USA

Abstract Greenland's glacial fjords are a key bottleneck in the earth system, regulating exchange of heat, freshwater and nutrients between the ice sheet and ocean and hosting societally important fisheries. We combine recent bathymetric, atmospheric, and oceanographic data with a buoyant plume model to show that summer subglacial discharge from 136 tidewater glaciers, amounting to 0.02 Sv of freshwater, drives 0.6–1.6 Sv of upwelling. Bathymetric analysis suggests that this is sufficient to renew most major fjords within a single summer, and that these fjords provide a path to the continental shelf that is deeper than 200 m for two-thirds of the glaciers. Our study provides a first pan-Greenland inventory of tidewater glacier fjords and quantifies regional and ice sheet-wide upwelling fluxes. This analysis provides important context for site-specific studies and is a step toward implementing fjord-scale heat, freshwater and nutrient fluxes in large-scale ice sheet and climate models.

Plain Language Summary The interaction between the Greenland Ice Sheet and the surrounding ocean is one of the key links in the regional climate system. Ocean heat melts the edges of the ice sheet, causing glacier speed-up, retreat and sea level contribution. Meltwater from the ice sheet enters the ocean where it alters ocean properties and potentially ocean currents. This meltwater also drives upwelling of nutrients that can impact local ecosystems. All of these processes occur in long, deep and narrow fjords that connect the ice sheet and ocean. In this study, we present a first continent-wide overview of the geometry and dynamics of Greenland's fjords. We combine recent bathymetric, atmospheric, and oceanographic datasets with a simple model to show that many fjords are well connected to the ocean in both bathymetry and circulation, suggesting that changes in the ocean on the continental shelf will be quickly transmitted to the ice sheet margin. We also suggest that meltwater from the ice sheet is rapidly mixed within fjords and will enter the wider ocean as a dilute subsurface mixture. This study is a step toward implementing fjord heat, freshwater and nutrient fluxes into large-scale models that cannot resolve fjords.

1. Introduction

The Greenland Ice Sheet interacts with the ocean through glacial fjords, which play a key role in moderating multiple components of the regional climate and ecosystem. Fjord-scale transport of ocean heat melts the termini of tidewater glaciers (Sutherland et al., 2019; Wood et al., 2021) in a process understood to have driven half of the ice sheet's mass loss since 1992 (Straneo & Heimbach, 2013; The IMBIE Team, 2020). Freshwater fluxed into the ocean from the ice sheet drives fjord circulation and stratification (Straneo et al., 2011) and enters Greenland's boundary currents and potentially the deep ocean (Böning et al., 2016; Dukhovskoy et al., 2019; Le Bras et al., 2021). Upwelling of deep nutrients in glacial fjords sustains higher productivity marine ecosystems than is typically observed in similar environments receiving only surface runoff (Hopwood et al., 2020), impacting inshore fisheries (Meire et al., 2017). Yet, across each of these disciplines, many of the processes and impacts remain poorly quantified on a pan-Greenland scale.

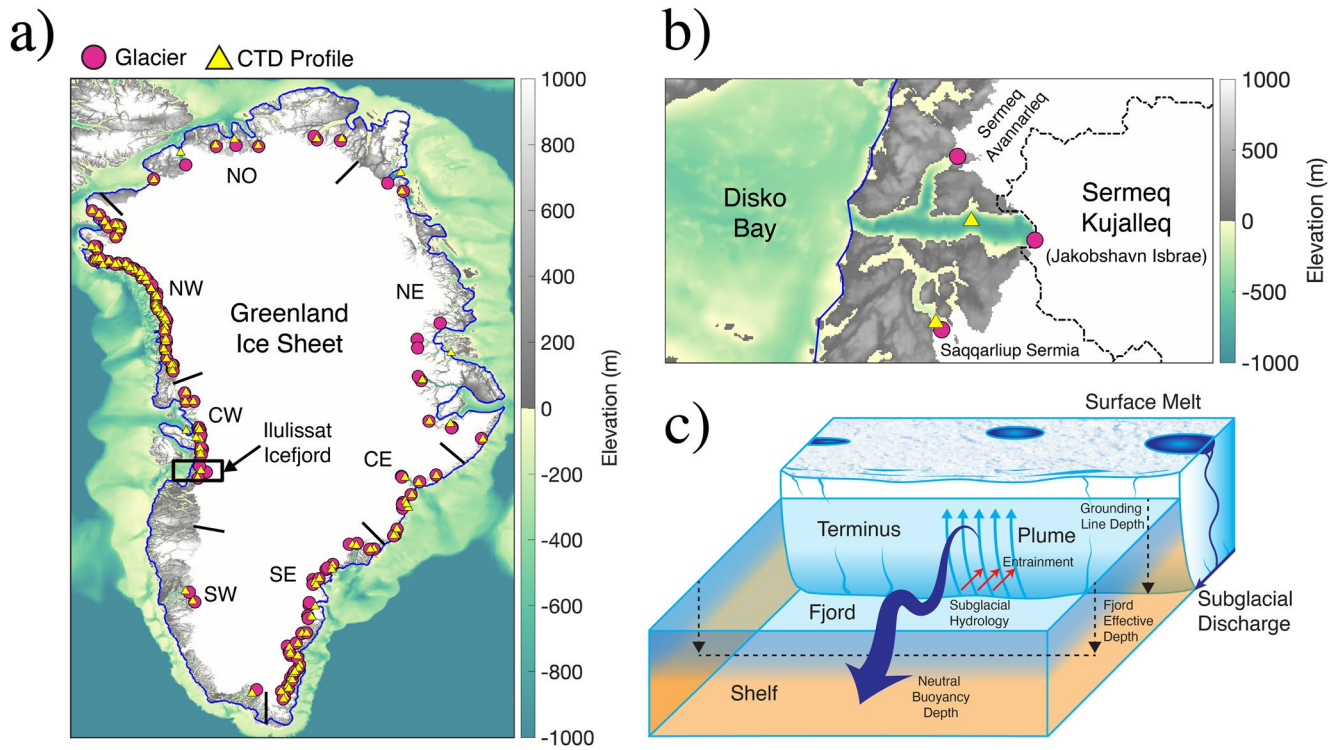

Figure 1. (a) Location of the 136 tidewater glaciers considered (purple circles) and the hydrographic profiles used to force the plume model (yellow triangles). The encompassing blue line defines the fjord-ocean boundary as described in Section 2.1. (b) Detail of the Ilulissat Isfjord system, containing three of the tidewater glaciers in our data set and the location of the conductivity-temperature-depth profile used to force the plume model at these glaciers. The dashed black line on the ice sheet denotes the boundaries of the hydrological catchment, over which surface meltwater drains to the bed and flows downstream to the grounding line of Sermeq Kujalleq. (c) Schematic of the glacier-plume-fjord system illustrating key definitions.

Greenland's ice sheet-ocean system consists of hundreds of tidewater glaciers connected to the continental shelf by almost as many glacial fjords (Figure 1). Each glacier delivers freshwater to the fjord in both iceberg and liquid form. The liquid freshwater is derived from submarine melting of the ice-ocean interface and, during summer, melting of the ice sheet surface (Figure 1c). Surface meltwater drains to the bed and enters the fjord at the grounding line as subglacial discharge, often hundreds of meters below the fjord surface. This process drives buoyant upwelling plumes that entrain ambient waters and reach neutral buoyancy in the stratified upper water column (Figure 1c; Jackson et al., 2017; Mankoff et al., 2016; Stevens et al., 2016). Among the many drivers of fjord circulation, such as variability in shelf water masses, winds, tides, sea-ice and icebergs (Davison et al., 2020; Jackson et al., 2014; Mortensen et al., 2014), the buoyancy-driven circulation induced by plumes during summer plays a key role in fluxing heat toward the ice sheet, freshwater toward the ocean, and deep nutrients into the euphotic zone (Beaird et al., 2018; Cape et al., 2019; Cowton et al., 2016; Oliver et al., 2020; Zhao et al., 2021).

Field observations from multiple fjords have shown that the total flux upwelled by a plume exceeds the subglacial discharge by 1–2 orders of magnitude and that after reaching neutral buoyancy, waters from the plume flow down-fjord in the subsurface (Beaird et al., 2018; Jackson et al., 2017; Mankoff et al., 2016). Numerical models have furthermore quantified how plume dynamics depend on grounding line depth, subglacial discharge and fjord stratification (De Andrés et al., 2020; Jenkins, 2011; Xu et al., 2013). A few studies have considered multiple glaciers: Carroll et al. (2016) evaluated plume dynamics and the induced submarine melting across 12 glaciers around the ice sheet, while Millan et al. (2018) showed that the majority of 20 examined glaciers in southeast Greenland have a deep connection to the continental shelf. Yet, to date there has not been a pan-Greenland examination of plume dynamics, fjord volumes and fjord-to-shelf connectivity, making it difficult to place individual fjord studies into an ice sheet-wide context. We also currently lack estimates of regional and ice sheet-wide plume fluxes and a quantification of how many glaciers have deep connections to the continental shelf. Such an aim has recently become achievable through new bathymetric and oceanographic datasets. Here, we therefore describe the first ice sheet-scale overview of fjord and plume characteristic depths, fluxes and renewal timescales.

2. Methods

2.1. Fjord and Glacier Delineation

We first delineate Greenland's tidewater glacier fjords using an algorithm based on the BedMachine v4 ice-ocean-land mask (Morlighem et al., 2021). We use the MATLAB function "*boundary*" to draw a boundary such that all mainland ice and land is contained within the boundary and define fjords as the collection of ocean pixels inside the boundary (Figure 1). The boundary has an associated "shrink factor" (α) that controls how tightly the boundary fits: $\alpha = 0$ corresponds to the convex hull (i.e., a loose fit) while $\alpha = 1$ yields the shoreline itself (i.e., a tight fit). The shrink factor controls the scale of topographic features that are considered to be a fjord, and its value is therefore subjective. A practical definition is to choose α such that the boundary separates regions that are typically resolved by large-scale ocean models (e.g., Disko Bay) and those that are not (e.g., narrow fjords). We set $\alpha = 0.5$, which results in Ilulissat Isfjord being considered a fjord (Figure 1b), while the outer part of Scoresby Sund is not (Figure 1a). Individual fjord systems (Figure 1b, Supporting Information S2) are then identified by grouping connected ocean pixels inside the boundary.

To define the tidewater glacier dataset, we use a list of Greenland's 243 fastest-flowing glaciers (Morlighem et al., 2017), but remove glaciers that: (a) have a grounding line depth shallower than 50 m according to BedMachine v4 (92 glaciers), (b) have a mean annual subglacial discharge less than 2.5 m^3s^{-1} (Section 2.2; seven glaciers), or (c) have a deepest path to the ocean that is shallower than 25 m (8 glaciers). By these criteria we focus on large tidewater glaciers with substantial upwelling that are well connected to the ocean. Each glacier is then allocated to its respective fjord. The resulting dataset contains 136 tidewater glaciers that drain into 89 fjords. A map and key statistics for each system are provided in Supporting Information S2 and S3.

2.2. Buoyant Plume Model and Inputs

We use the buoyant plume model described in Slater et al. (2016) without modification to quantify upwelling driven by subglacial discharge at tidewater glaciers. Relative to a full numerical ocean model, buoyant plume models are more practical for simulating hundreds of plumes and perform well in idealized scenarios such as are considered here (Kimura et al., 2014). Plume models are furthermore increasingly well-validated by studies comparing observed and simulated fluxes and characteristic depths (De Andrés et al., 2020; Jackson et al., 2017). Following studies suggesting that a line plume geometry of a few hundred meters width best captures near-glacier observations (Fried et al., 2019; Jackson et al., 2017), we employ a line plume model with width of $w = 250$ m.

For inputs, the plume model requires subglacial discharge and fjord temperature and salinity profiles. The subglacial discharge dataset is from Mankoff et al. (2020) and we consider a single value of subglacial discharge for each glacier that is the mean summer (June, July, August) value during 2010–2020. Fjord hydrography is provided by shipboard and airborne conductivity-temperature-depth profiles collected between July and October during 2013–2020 (Fenty et al., 2016; Mankoff et al., 2016; Mortensen et al., 2020; Willis et al., 2018, Figure S1 in Supporting Information S1). To each tidewater glacier we assign the closest profile (Figures 1a and 1b), so that 102 (out of 136) glaciers have a profile from within 10 km of the terminus (Figures 1 and S1 in Supporting Information S1), 131 have a profile within 50 km and all but four glaciers have a profile within their associated fjord.

2.3. Sensitivity Experiments

Recognizing that the distribution of subglacial discharge at grounding lines is poorly constrained by observations, we conduct sensitivity experiments with small ($w = 100$ m) and large ($w = 500$ m) plume widths. From a plume model perspective, a single plume of width 500 m is identical to two plumes of width 250 m, so our analysis implicitly includes the possibility of multiple plumes at a single glacier. We also assess the impact of temporal variability in summer subglacial discharge by running the model with low and high values of subglacial discharge that are respectively the minimum and maximum summer discharge months for each glacier over the 2010–2020 period. The dominant plume model parameter that controls fluxes is the entrainment coefficient; here we assume a value of 0.1 (Slater et al., 2016) but, recognizing uncertainty in this value, also consider values of 0.05 and 0.15 (e.g., Kimura et al., 2014).

We also quantify the impact of temporal variability in fjord stratification on plumes for two major systems: Helheim Gletsjer and Kangilliup Sermia (Rink Isbræ). The wealth of observations from the associated fjords

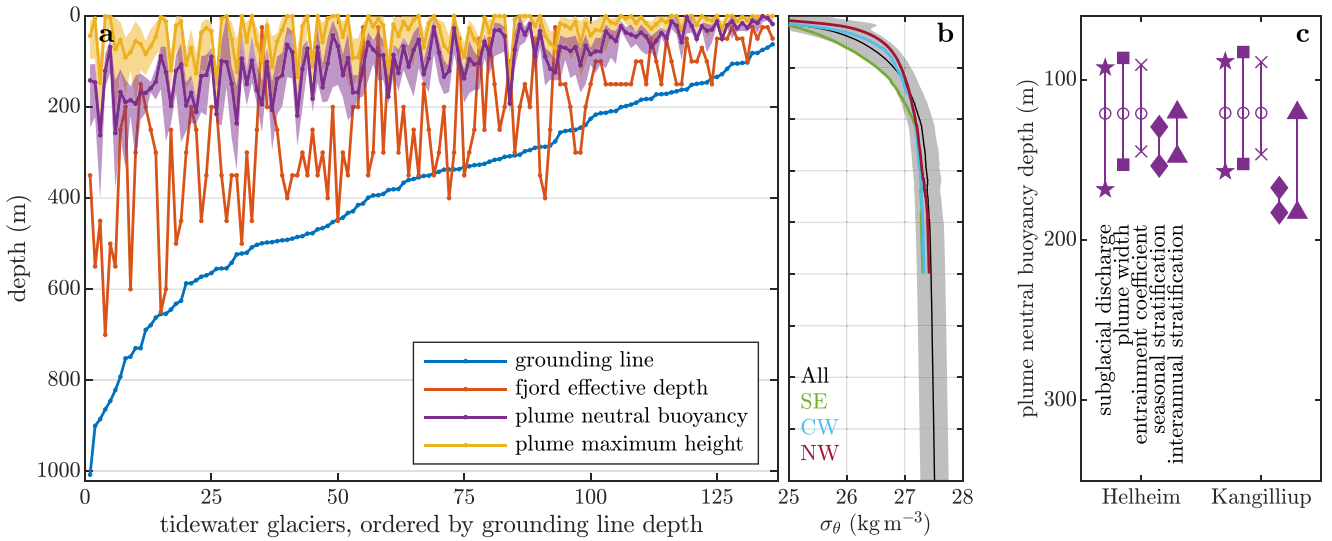

Figure 2. (a) Characteristic depths for Greenland's tidewater glacier fjords, sorted by grounding line depth. The shading on neutral buoyancy and maximum height shows the range arising from variation in subglacial discharge, plume width and entrainment coefficient. (b) Observed fjord potential density anomaly, showing the mean and standard deviation for all casts (black and shading), and the mean for the three regions containing the most tidewater glaciers (SE, CW and NW). (c) Focus on Helheim Gletsjer, SE Greenland and Kangilliup Sermia (Rink Isbræ), west Greenland, showing the range in plume neutral buoyancy depth arising from variability in subglacial discharge, plume width, entrainment coefficient and fjord stratification. Hollow circles show central values as on (a). Note the different *y*-axis scale on (c).

(e.g., Carroll et al., 2018; Straneo et al., 2011) allows us to consider seasonal variability (by comparing plumes in early- and late-summer stratification) and interannual variability (by comparing plumes experiencing stratification from different years). Further details on the observations used are given in Figure S5 in Supporting Information S1.

2.4. Definitions

This study centers around several key quantities (Figure 1) that require definition. The plume is assumed to originate at the *grounding line depth*, defined as the maximum depth of the calving front from BedMachine v4 (Morlighem et al., 2021). The *fjord effective depth* is the depth of the deepest water on the continental shelf at the fjord mouth that can access the glacier without being impeded by bathymetry. The fjord effective depth may correspond to a sill depth, or may be the depth of the shelf itself if the entire fjord is deeper than the shelf. As buoyant plumes rise, there comes a depth where the density of waters in the plume equals that of the ambient stratification (e.g., Figure S5 in Supporting Information S1), termed the *plume neutral buoyancy depth*. Due to inertia, the plume will overshoot this depth until it stops rising at the *plume maximum height*. We neglect the dynamics of plumes beyond their maximum height, for example, rebound and flow away from the glacier, but revisit this limitation in the discussion. As such, we use the plume neutral buoyancy depth as an estimate of the depth at which the plume will flow horizontally away from the glacier.

The *upwelling flux* is defined as the plume volume flux at the neutral buoyancy depth, providing an estimate of the summer upwelling by a tidewater glacier. Lastly, the *plume-driven renewal time* is defined as the ratio of the fjord volume below the neutral buoyancy depth to the upwelling flux. The fjord volume is calculated based on the bathymetry and the algorithmic delineation of each fjord as described above. Where multiple glaciers (and plumes) exist in a fjord, we calculate volume on the basis of the shallowest plume's neutral buoyancy and flux as the sum of the individual upwelling fluxes. The plume-driven renewal time is thus a simple estimate, in isolation of all other processes, of how long it would take the plume to upwell/renew all of the deep waters in the fjord.

3. Results

Considering first characteristic depths, grounding lines vary between 1,000 and 60 m, while fjord effective depths range from 700 to 25 m with an interquartile range of 350 to 100 m (Figure 2a). Plumes rise unimpeded through weakly stratified deep water but are trapped in the subsurface by light ambient waters close to the surface

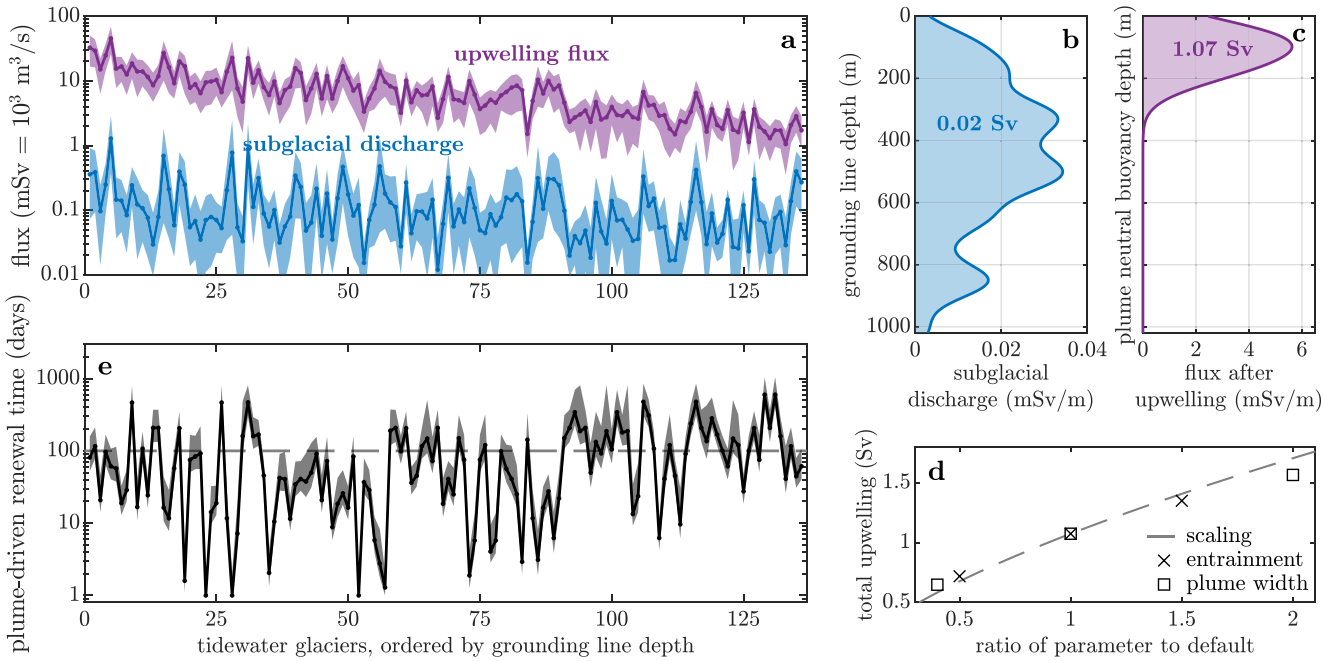

Figure 3. (a) Summer subglacial discharge and upwelling flux for Greenland's tidewater glaciers. (b) Kernel probability distribution function for subglacial discharge versus grounding line depth and for (c) volume flux after upwelling versus neutral buoyancy depth. Values inside the shading in (b) and (c) give the total depth-integrated flux. (d) Total upwelling as a function of assumed plume width and entrainment coefficient. (e) Plume-driven renewal time. Glacier/fjord systems that fall below the gray dashed line have a renewal time of less than 100 days and can renew within a single summer. The shading in (a) and (e) shows the range arising from variation in subglacial discharge, plume width and entrainment coefficient.

(Figure 2b), so that plume neutral buoyancy depths range from 260 to 0 m with an interquartile range of 130 to 50 m and plume maximum height ranges from 150 to 0 m with an interquartile range of 60 to 0 m (Figures 2a and S2 in Supporting Information S1). Characteristic depths are related; for example, grounding line depth explains 55% of variability in neutral buoyancy depth and, on average, plumes equilibrate 22 m deeper for every 100 m of grounding line depth (Figure S3 in Supporting Information S1).

By focusing on Helheim Gletsjer we can explore the dominant sources of variability and uncertainty in calculated plume neutral buoyancy. Holding stratification fixed, monthly variability in summer subglacial discharge can drive excursions of 80 m in plume neutral buoyancy depth (Figures 2c and S5 in Supporting Information S1). Adopting the narrow or wide plume width gives a range of 70 m, while changing the entrainment coefficient by 50% gives a range of 50 m. With fixed discharge, the stratification observed in March and August 2010 yields a difference in neutral buoyancy depth of 30 m, while use of late summer stratification from each of the years 2008–2012 causes neutral buoyancy to vary by 30 m. Similar magnitudes of variability are obtained for Kangilliup Sermia (Figures 2c and S5 in Supporting Information S1). Since for these two glaciers the range in plume neutral buoyancy obtained by varying discharge or model parameters is much larger than that arising from temporal variability in stratification, we consider it justified to use synoptic ocean profiles for the other glaciers in our analysis. Note that we are not suggesting neutral buoyancy does not vary seasonally, only commenting on the relative importance of difference sources of variability in our analysis.

Entrainment of ambient water into the energetic plumes ensures that subglacial discharge of 0.01–1 mSv (10–10^3 m^3s^{-1}) per glacier drives upwelling amounting to 1–45 mSv (Figure 3a), which is consistent with field observations (Jackson et al., 2017; Mankoff et al., 2016). The upwelling flux responds to both the magnitude of subglacial discharge and the grounding line depth (Straneo & Cenedese, 2015), the latter due to the greater distance over which the rising plume entrains ambient water (Figure 3a). Considering all glaciers together, the emergence of fresh subglacial discharge from glacier grounding lines amounts to 0.02 Sv that is relatively uniformly spread over 0–1,000 m depth (Figure 3b). The resulting plumes, however, drive an upwelling flux of 1.07 Sv, approximately two orders of magnitude greater, that equilibrates primarily at 50–200 m depth (Figure 3c). Monthly variability in summer subglacial discharge leads to a minimum upwelling flux of 0.55 Sv in June 2018

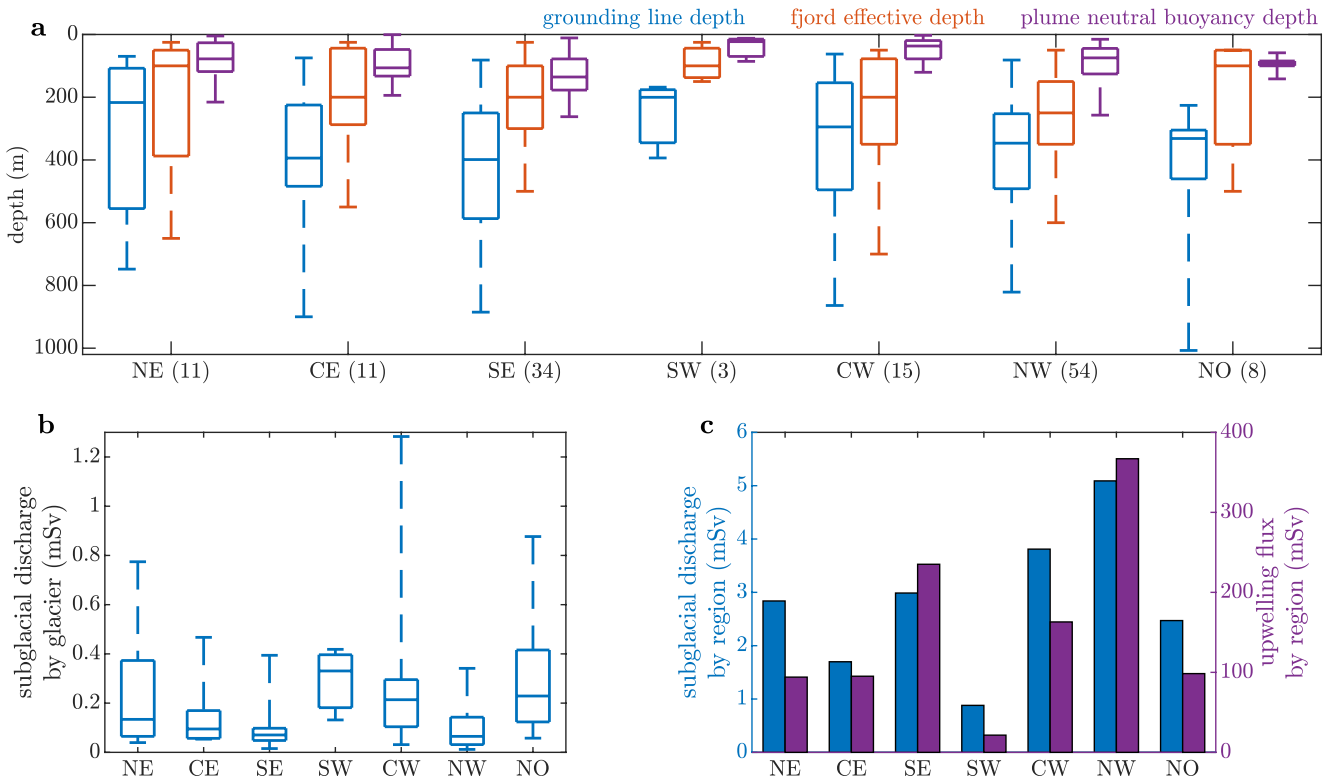

Figure 4. (a) Box and whiskers plot for characteristic depths grouped by the regions shown in Figure 1a. The bracketed numbers on the *x*-axis show the number of glaciers per region in our dataset. (b) Subglacial discharge per glacier. (c) Total subglacial discharge (blue, left axis) and upwelling flux (purple, right axis) by region.

and a maximum upwelling flux of 1.55 Sv in July 2012. Adopting the narrow or wide plume width changes the upwelling flux to 0.65 or 1.57 Sv, respectively, while varying the entrainment coefficient yields a range of 0.72–1.35 Sv (Figure 3d). The sensitivity of upwelling flux to plume width and the entrainment coefficient is in general agreement with the 2/3 power law expected from theory (Jenkins, 2011). For the central values of all parameters, the plume-driven renewal time is less than 100 days for 62 out of 89 fjords (corresponding to 85 out of 136 glaciers), indicating that subglacial discharge-driven plumes can renew most major fjords during a single summer (Figure 3e).

No region is statistically distinct in grounding line depth when compared against all others using a two-sample Kolmogorov-Smirnov test (Figures 4a and S6 in Supporting Information S1). For plume neutral buoyancy depth, however, the SE and CW regions are statistically distinct. In SE Greenland, the median neutral buoyancy depth of 136 m is deeper than the ice sheet-wide median of 86 m, due to SE Greenland having relatively deep grounding lines (Figure 4a), low subglacial discharge (Figure 4b) and a more stratified water column (Figure 2b). CW Greenland, with a median of 37 m, has shallower plume neutral buoyancy than the rest of the ice sheet (Figure 4a) due to shallow grounding lines, high subglacial discharge and a more weakly stratified water column (Figure 2b). We caution against lending too much weight to regional comparisons in stratification, however, since not all regions were sampled simultaneously (Figure S1 in Supporting Information S1), so we are not able to isolate regional versus temporal variability in stratification. The SE, CW, and NW are the dominant regions in terms of total subglacial discharge and upwelling due to their large number of tidewater glaciers (Figure 4c). Note that upwelling flux depends on subglacial discharge but also on grounding line depth, explaining why some regions can have relatively high subglacial discharge but lower upwelling.

4. Discussion

We have presented a first ice sheet-wide assessment of the depths and fluxes that characterize summer subglacial discharge-driven upwelling in Greenland's tidewater glacier fjords. We find that just 0.02 Sv of subglacial discharge distributed approximately uniformly over depth drives 0.6–1.6 Sv of upwelling that reaches neutral

buoyancy at 0–260 m depth, renewing most fjords within a single summer (Figures 2 and 3). While SE, CW and NW Greenland are the dominant regions in subglacial discharge and upwelling flux (Figure 4), just the 10 glaciers with the highest subglacial discharge account for 31% of the total subglacial discharge from all 136 glaciers. Similarly, the 10 glaciers with the highest upwelling flux account of 24% of the total upwelling. Sermeq Kujalleq (Jakobshavn Isbræ) is notable as the single largest contributor to upwelling, alone accounting for 4% of the total.

Observations from fjord case studies, while limited, support our principal conclusions. Mankoff et al. (2016), Jackson et al. (2017) and De Andrés et al. (2020) matched observed and modeled plume depths and fluxes in west Greenland fjords. These studies showed plumes equilibrating in the subsurface and high upwelling fluxes, consistent with results from the same plume model used here. In Sermilik Fjord, SE Greenland, Beaird et al. (2018) estimated a glacially modified water export of 74 mSv over the top 200 m of the water column, containing 800 $\pm$ 500 m^3s^{-1} of subglacial discharge. Our discharge estimate of 140–960 m^3s^{-1} and plume neutral buoyancy depth of 86–213 m are in a similar range, but our plume upwelling flux of 18–47 mSv is 2–5 times smaller than the observed export flux. Muilwijk et al. (2022) have similarly estimated that in Upernavik Fjord, plume upwelling comprises only around 60% of the exported water mass. These studies highlight the importance of fjord-scale mixing processes beyond the plume, including lateral recirculation, winds, tides, flow-topography interactions and iceberg-driven mixing (Beaird et al., 2018; Carroll et al., 2017; Mortensen et al., 2014; Slater et al., 2018; Straneo & Cenedese, 2015). The upwelling fluxes presented here are therefore likely to provide a lower bound on the export flux from fjords to the ocean. Numerical ocean models however suggest that, despite further mixing, the plume neutral buoyancy depth remains a good estimate of the depth at which export to the ocean occurs (Carroll et al., 2015, 2017).

A number of further limitations should be considered and provide a focus for future efforts. First, the distribution of subglacial discharge at grounding lines, including the possibility for multiple plumes, is poorly constrained by observations. This uncertainty is represented in our analysis by variable plume width, which strongly affects the plume neutral buoyancy depth, upwelling flux and plume-driven renewal time (Figures 2 and 3). Second, we have largely relied on synoptic hydrographic profiles from fjords that may show significant temporal variability, and previous work has shown that this can affect plume dynamics (De Andrés et al., 2020; Podolskiy et al., 2021). Third, our analysis accounts for only 13% of the total ice sheet freshwater flux over the 2010–2020 period. The other significant terms are solid ice discharge (50%), subglacial discharge from land-terminating margins (28%) and subglacial discharge from tidewater glaciers not included in our analysis (7%; Figure S7 in Supporting Information S1). While our analysis accounts for the vast majority of upwelling around the ice sheet, fully characterizing Greenland's freshwater input to the ocean requires additional consideration of the non-summer months, of icebergs and of runoff from land and groundwater.

Despite these limitations, our study has a number of key implications. In terms of impact on the ice sheet, the quantification of fjord effective depth identifies the depth range of inflowing shelf water masses that drive submarine melting of tidewater glaciers. The vast majority of grounding lines are deeper than the fjord effective depth (Figure 2a), meaning that most fjords either have a sill or are deeper than the continental shelf. Yet, 82 of 136 glaciers are in fjords with effective depth deeper than 200 m, indicating that warm dense waters on the continental shelf can readily access most glacier grounding lines, a finding that is consistent with previous regional or site-specific studies (e.g., Millan et al., 2018; Straneo et al., 2010). The remaining 54 glaciers are protected from, or may experience less frequent incursions of warm shelf waters, but are typically small glaciers with shallow grounding lines. In the absence of a more complete approach for ocean forcing of an ice sheet model, the water masses melting the ice sheet might reasonably be taken as the water masses on the continental shelf at the fjord effective depths estimated in this study.

In terms of impact on the ocean, and subject to the caveats described above, the plume neutral buoyancy depth sets the depth for export of glacially modified water to the shelf. Our results suggest that over half is exported below 100 m depth (Figure 3c), a fact that should be represented in ocean models examining the impact of Greenland freshwater on the ocean. Indeed, the upwelling fluxes quantified here could be combined with estimates of mixing in fjords beyond the plume (Beaird et al., 2018; Muilwijk et al., 2022) to provide boundary conditions for large-scale ocean models that do not resolve fjords. Finally, plumes may impact fjord primary productivity if upwelling reaches into the photic zone, which has a typical depth of at most 50 m (Mascarenhas & Zielinski, 2019; Meire et al., 2017). Only 28% of glaciers considered here have plumes reaching neutral buoyancy in

the photic zone, though it is 72% if we consider plume maximum height (Figure 2). For the maximum subglacial discharge, these fractions increase to 46% and 87%, respectively, though we note that these fractions neglect the finite vertical extent of plume waters flowing away from the glacier. Based on plume upwelling alone then, it is mostly the glaciers with shallower grounding lines that will influence productivity throughout summer, but we note that vertical mixing in the fjord beyond the plume may transport upwelled nutrients into the photic zone.

5. Summary

Greenland's fjords play a critical role connecting the ice sheet, ocean and marine ecosystems. We find that fjords provide a path to the ocean that is sufficiently deep to allow warm waters to access the majority of large tidewater glaciers. During summer, just 0.02 Sv of total subglacial discharge drives 0.6–1.6 Sv of upwelling, sufficient to renew most fjords within a single summer. The neutral buoyancy depth of the upwelled water, spanning 0–260 m, sets the depth for export of glacially modified waters to the continental shelf. We anticipate that the mapping of characteristic depths and fluxes for Greenland's glacial fjords undertaken here will provide important context for site-specific studies and be useful across multiple fields of ice-ocean-ecosystem research.

Data Availability Statement

All data and code required to reproduce this research, together with the outputs and plotting scripts are available at https://doi.org/10.5281/zenodo.6498180 or https://github.com/donaldaslater/fjords_GRL_2022/.

Acknowledgments
DAS acknowledges support from NERC Independent Research Fellowship NE/T011920/1. DAS and FS acknowledge support from NSF award 2020547. HO acknowledges support from a WHOI Postdoctoral Scholar award. MW and JKW performed this work at the Jet Propulsion Laboratory, California Institute of Technology, under contract with the National Aeronautics and Space Administration. MM is an editor of the journal.

References

Beaird, N. L., Straneo, F., & Jenkins, W. (2018). Export of strongly diluted Greenland meltwater from a major glacial fjord. *Geophysical Research Letters*, *45*(9), 4163–4170. https://doi.org/10.1029/2018GL077000

Böning, C. W., Behrens, E., Biastoch, A., Getzlaff, K., & Bamber, J. L. (2016). Emerging impact of Greenland meltwater on deepwater formation in the North Atlantic Ocean. *Nature Geoscience*, *9*(7), 523–527. https://doi.org/10.1038/ngeo2740

Cape, M. R., Straneo, F., Beaird, N., Bundy, R. M., & Charette, M. A. (2019). Nutrient release to oceans from buoyancy-driven upwelling at Greenland tidewater glaciers. *Nature Geoscience*, *12*(1), 34–39. https://doi.org/10.1038/s41561-018-0268-4

Carroll, D., Sutherland, D. A., Curry, B., Nash, J. D., Shroyer, E. L., Catania, G. A., et al. (2018). Subannual and seasonal variability of Atlantic-origin waters in two adjacent west Greenland fjords. *Journal of Geophysical Research: Oceans*, *123*(9), 6670–6687. https://doi.org/10.1029/2018JC014278

Carroll, D., Sutherland, D. A., Hudson, B., Moon, T., Catania, G. A., Shroyer, E. L., et al. (2016). The impact of glacier geometry on meltwater plume structure and submarine melt in Greenland fjords. *Geophysical Research Letters*, *43*(18), 9739–9748. https://doi.org/10.1002/2016GL070170

Carroll, D., Sutherland, D. A., Shroyer, E. L., Nash, J. D., Catania, G. A., & Stearns, L. A. (2015). Modeling turbulent subglacial meltwater plumes: Implications for fjord-scale buoyancy-driven circulation. *Journal of Physical Oceanography*, *45*(8), 2169–2185. https://doi.org/10.1175/JPO-D-15-0033.1

Carroll, D., Sutherland, D. A., Shroyer, E. L., Nash, J. D., Catania, G. A., & Stearns, L. A. (2017). Subglacial discharge-driven renewal of tidewater glacier fjords. *Journal of Geophysical Research: Oceans*, *122*(8), 6611–6629. https://doi.org/10.1002/2017JC012962

Cowton, T., Sole, A., Nienow, P., Slater, D., Wilton, D., & Hanna, E. (2016). Controls on the transport of oceanic heat to Kangerdlugssuaq glacier, East Greenland. *Journal of Glaciology*, *62*(236), 1167–1180. https://doi.org/10.1017/jog.2016.117

Davison, B. J., Cowton, T. R., Cottier, F. R., & Sole, A. J. (2020). Iceberg melting substantially modifies oceanic heat flux towards a major Greenlandic tidewater glacier. *Nature Communications*, *11*(5983). https://doi.org/10.1038/s41467-020-19805-7

De Andrés, E., Slater, D. A., Straneo, F., Otero, J., Das, S., & Navarro, F. (2020). Surface emergence of glacial plumes determined by fjord stratification. *The Cryosphere*, *14*(6), 1951–1969. https://doi.org/10.5194/tc-14-1951-2020

Dukhovskoy, D. S., Yashayaev, I., Proshutinsky, A., Bamber, J. L., Bashmachnikov, I. L., Chassignet, E. P., et al. (2019). Role of Greenland freshwater anomaly in the recent freshening of the subpolar North Atlantic. *Journal of Geophysical Research: Oceans*, *124*(5), 3333–3360. https://doi.org/10.1029/2018JC014686

Fenty, I., Willis, J. K., Khazendar, A., Dinardo, S., Forsberg, R., Fukumori, I., et al. (2016). Oceans melting Greenland: Early results from NASA's ocean-ice mission in Greenland. *Oceanography*, *29*(4), 72–83. https://doi.org/10.5670/oceanog.2016.100

Fried, M. J., Carroll, D., Catania, G. A., Sutherland, D. A., Stearns, L. A., Shroyer, E. L., & Nash, J. D. (2019). Distinct frontal ablation processes drive heterogeneous submarine terminus morphology. *Geophysical Research Letters*, *46*(21), 12083–12091. https://doi.org/10.1029/2019GL083980

Hopwood, M. J., Carroll, D., Dunse, T., Hodson, A., Holding, J. M., Iriarte, J. L., et al. (2020). Review article: How does glacier discharge affect marine biogeochemistry and primary production in the arctic? *The Cryosphere*, *14*(4), 1347–1383. https://doi.org/10.5194/tc-14-1347-2020

Jackson, R. H., Shroyer, E. L., Nash, J. D., Sutherland, D. A., Carroll, D., Fried, M. J., et al. (2017). Near-glacier surveying of a subglacial discharge plume: Implications for plume parameterizations. *Geophysical Research Letters*, *44*(13), 6886–6894. https://doi.org/10.1002/2017GL073602

Jackson, R. H., Straneo, F., & Sutherland, D. A. (2014). Externally forced fluctuations in ocean temperature at Greenland glaciers in non-summer months. *Nature Geoscience*, *7*(7), 503–508. https://doi.org/10.1038/ngeo2186

Jenkins, A. (2011). Convection-driven melting near the grounding lines of ice shelves and tidewater glaciers. *Journal of Physical Oceanography*, *41*(12), 2279–2294. https://doi.org/10.1175/JPO-D-11-03.1

Kimura, S., Holland, P. R., Jenkins, A., & Piggot, M. (2014). The effect of meltwater plumes on the melting of a vertical glacier face. *Journal of Physical Oceanography*, *44*(12), 3099–3117. https://doi.org/10.1175/JPO-D-13-0219.1

Le Bras, I., Straneo, F., Muilwijk, M., Smedsrud, L. H., Li, F., Lozier, M. S., & Holliday, N. P. (2021). How much arctic fresh water participates in the subpolar overturning circulation? *Journal of Physical Oceanography*, *51*(3), 955–973. https://doi.org/10.1175/JPO-D-20-0240.1

Mankoff, K. D., Noël, B., Fettweis, X., Ahlstrøm, A. P., Colgan, W., Kondo, K., et al. (2020). Greenland liquid water discharge from 1958 through 2019. *Earth System Science Data*, *12*(4), 2811–2841. https://doi.org/10.5194/essd-12-2811-2020

Mankoff, K. D., Straneo, F., Cenedese, C., Das, S. B., Richards, C. G., & Singh, H. (2016). Structure and dynamics of a subglacial discharge plume in a Greenlandic fjord. *Journal of Geophysical Research: Oceans*, *121*(12), 8670–8688. https://doi.org/10.1002/2016JC011764

Mascarenhas, V. J., & Zielinski, O. (2019). Hydrography-driven optical domains in the vaigat-disko bay and godthabsfjord: Effects of glacial meltwater discharge. *Frontiers in Marine Science*, *6*. https://doi.org/10.3389/fmars.2019.00335

Meire, L., Mortensen, J., Meire, P., Juul-Pedersen, T., Sejr, M. K., Rysgaard, S., et al. (2017). Marine-terminating glaciers sustain high productivity in Greenland fjords. *Global Change Biology*, *23*(12), 5344–5357. https://doi.org/10.1111/gcb.13801

Millan, R., Rignot, E., Mouginot, J., Wood, M., Bjørk, A. A., & Morlighem, M. (2018). Vulnerability of southeast Greenland glaciers to warm Atlantic water from operation icebridge and ocean melting Greenland data. *Geophysical Research Letters*, *45*(6), 2688–2696. https://doi.org/10.1002/2017GL076561

Morlighem, M., Williams, C. N., Rignot, E., An, L., Arndt, J. E., Bamber, J. L., et al. (2017). Bedmachine v3: Complete bed topography and ocean bathymetry mapping of Greenland from multibeam echo sounding combined with mass conservation. *Geophysical Research Letters*, *44*(21), 51–111. https://doi.org/10.1002/2017GL074954

Morlighem, M., Williams, C. N., Rignot, E., An, L., Arndt, J. E., Bamber, J. L., & Zinglersen, K. B. (2021). *Icebridge bedmachine Greenland, version 4. NASA National Snow and Ice Data Center distributed active archive center*. https://doi.org/10.5067/VLJ5YXKCNGXO

Mortensen, J., Bendtsen, J., Lennert, K., & Rysgaard, S. (2014). Seasonal variability of the circulation system in a West Greenland tidewater outlet glacier fjord, Godthabsfjord (64N). *Journal of Geophysical Research: Earth Surface*, *119*(12), 2591–2603. https://doi.org/10.1002/2014JF003267

Mortensen, J., Rysgaard, S., Bendtsen, J., Lennert, K., Kanzow, T., Lund, H., & Meire, L. (2020). Subglacial discharge and its down-fjord transformation in west Greenland fjords with an ice melange. *Journal of Geophysical Research: Oceans*, *125*(9), e2020JC016301. https://doi.org/10.1029/2020JC016301

Muilwijk, M., Straneo, F., Slater, D. A., Smedsrud, L. H., Holte, J., Wood, M., et al. (2022). Export of ice sheet meltwater from upernavik fjord, west Greenland. *Journal of Physical Oceanography*, *52*(3), 363–382. https://doi.org/10.1175/JPO-D-21-0084.1

Oliver, H., Castelao, R. M., Wang, C., & Yager, P. L. (2020). Meltwater-enhanced nutrient export from Greenland's glacial fjords: A sensitivity analysis. *Journal of Geophysical Research: Oceans*, *125*(7), e2020JC016185. https://doi.org/10.1029/2020JC016185

Podolskiy, E. A., Kanna, N., & Sugiyama, S. (2021). Co-seismic eruption and intermittent turbulence of a subglacial discharge plume revealed by continuous subsurface observations in Greenland. *Nature Communications Earth & Environment*, *2*(1), 66. https://doi.org/10.1038/s43247-021-00132-8

Slater, D. A., Goldberg, D. N., Nienow, P. W., & Cowton, T. R. (2016). Scalings for submarine melting at tidewater glaciers from buoyant plume theory. *Journal of Physical Oceanography*, *46*(6), 1839–1855. https://doi.org/10.1175/JPO-D-15-0132.1

Slater, D. A., Straneo, F., Das, S. B., Richards, C. G., Wagner, T. J. W., & Nienow, P. W. (2018). Localized plumes drive front-wide ocean melting of a Greenlandic tidewater glacier. *Geophysical Research Letters*, *45*(22), 12350–12358. https://doi.org/10.1029/2018GL080763

Stevens, L. A., Straneo, F., Das, S. B., Plueddemann, A. J., Kukulya, A. L., & Morlighem, M. (2016). Linking glacially modified waters to catchment-scale subglacial discharge using autonomous underwater vehicle observations. *The Cryosphere*, *10*(1), 417–432. https://doi.org/10.5194/tc-10-417-2016

Straneo, F., & Cenedese, C. (2015). The dynamics of Greenland's glacial fjords and their role in climate. *Annual Reviews of Marine Science*, *7*(1), 89–112. https://doi.org/10.1146/annurev-marine-010213-135133

Straneo, F., Curry, R. G., Sutherland, D. A., Hamilton, G. S., Cenedese, C., Vage, K., & Stearns, L. A. (2011). Impact of fjord dynamics and glacial runoff on the circulation near Helheim Glacier. *Nature Geoscience*, *4*(5), 322–327. https://doi.org/10.1038/ngeo1109

Straneo, F., Hamilton, G. S., Sutherland, D. A., Stearns, L. A., Davidson, F., Hammill, M. O., et al. (2010). Rapid circulation of warm subtropical waters in a major glacial fjord in East Greenland. *Nature Geoscience*, *3*(3), 182–186. https://doi.org/10.1038/ngeo764

Straneo, F., & Heimbach, P. (2013). North Atlantic warming and the retreat of Greenland's outlet glaciers. *Nature*, *504*(7478), 36–43. https://doi.org/10.1038/nature12854

Sutherland, D. A., Jackson, R. H., Kienholz, C., Amundson, J. M., Dryer, W. P., Duncan, D., et al. (2019). Direct observations of submarine melt and subsurface geometry at a tidewater glacier. *Science*, *365*(6451), 369–374. https://doi.org/10.1126/science.aax3528

The IMBIE Team. (2020). Mass balance of the Greenland ice sheet from 1992 to 2018. *Nature*, *579*(7798), 233–239. https://doi.org/10.1038/s41586-019-1855-2

Willis, J. K., Carroll, D., Fenty, I., Kohli, G., Khazendar, A., Rutherford, M., et al. (2018). Ocean-ice interactions in inglefield gulf: Early results from NASA's oceans melting Greenland mission. *Oceanography*, *31*(2), 100–108. https://doi.org/10.5670/oceanog.2018.211

Wood, M., Rignot, E., Fenty, I., An, L., Bjørk, A., van den Broeke, M., et al. (2021). Ocean forcing drives glacier retreat in Greenland. *Science Advances*, *7*(1). https://doi.org/10.1126/sciadv.aba7282

Xu, Y., Rignot, E., Fenty, I., Menemenlis, D., & Flexas, M. M. (2013). Subaqueous melting of Store glacier, West Greenland from three-dimensional, high-resolution numerical modeling and ocean observations. *Geophysical Research Letters*, *40*(17), 4648–4653. https://doi.org/10.1002/grl.50825

Zhao, K. X., Stewart, A. L., & McWilliams, J. C. (2021). Geometric constraints on glacial fjord–shelf exchange. *Journal of Physical Oceanography*, *51*(4), 1223–1246. https://doi.org/10.1175/JPO-D-20-0091.1